ADVANCED MATERIALS

focal point of a germanium lens which directed thermal energy from a heat source 30 cm away onto the circuit board while also filtering out extraneous visible light. A multimeter (Keithley, model 2700) was used to record the changes in resistance of the films.

Film percentages by weight: PVA (60.0 %), PEG (24.3 %), XC72 (10.0 %), TlpA8 (4.3 %), and X-100 (1.4 %).

Received: July 3, 2003
Final version: January 16, 2004

[1] R. R. Naik, L. L. Brott, S. M. Kirkpatrick, M. O. Stone, *Proc. SPIE—Int. Soc. Opt. Eng.* **2001**, *4590*, 115.
[2] R. R. Naik, S. M. Kirkpatrick, M. O. Stone, *Biosens. Bioelectron.* **2001**, *16*, 1051.
[3] R. McKendry, J. Zhang, Y. Arntz, T. Strunz, M. Hegner, H. P. Lang, M. K. Baller, C. Ulrich, E. Meyer, H. J. Guntherodt, C. Gerber, *Proc. Natl. Acad. Sci. USA* **2002**, *99*, 9783.
[4] R. Hurme, K. D. Berndt, S. J. Normark, M. Rhen, *Cell* **1997**, *90*, 55.
[5] R. Hurme, K. D. Berndt, E. Namork, M. Rhen, *J. Biol. Chem.* **1996**, *271*, 12 626.
[6] U. Mayor, C. M. Johnson, V. Daggett, A. R. Fersht, *Proc. Natl. Acad. Sci. USA* **2000**, *97*, 13 518.
[7] G. Agarwal, R. R. Naik, M. O. Stone, *J. Am. Chem. Soc.* **2003**, *125*, 7408.
[8] D. X. Hammer, J. Seigert, M. O. Stone, H. G. Rylander III, A. J. Welch, *J. Insect Physiol.* **2001**, *47*, 1441.
[9] N. Fuchigami, J. Hazel, V. V. Gorbunov, M. Stone, M. Grace, V. V. Tsukruk, *Biomacromolecules* **2001**, *2*, 757.
[10] A. L. Campbell, R. R. Naik, L. Sowards, M. O. Stone, *Micron* **2002**, *33*, 211.
[11] M. Anker, M. Stading, A. Hermansson, *J. Agric. Food Chem.* **2001**, *49*, 989.
[12] J. J. G. Van Soest, N. Knooren, *J. Appl. Polym. Sci.* **1997**, *64*, 1411.
[13] F. Zee, J. W. Judy, *Sens. Actuators, B* **2001**, *72*, 120.
[14] A. R. Hopkins, N. S. Lewis, *Anal. Chem.* **2001**, *73*, 884.
[15] M. E. Koscho, R. H. Grubbs, N. S. Lewis, *Anal. Chem.* **2002**, *74*, 1307.
[16] V. D. Pham, *US Patent 5 977 862*, **1999**.
[17] P. Tangboriboonrat, C. Rakdee, *J. Appl. Polym. Sci.* **2001**, *82*, 489.
[18] P. Gruenewald, J. S. Cashmore, J. Fieret, M. C. Gower, *Proc. SPIE—Int. Soc. Opt. Eng.* **2001**, *4274*, 158.
[19] M. Narkis, A. Ram, Z. Stein, *J. Appl. Polym. Sci.* **1980**, *25*, 1515.
[20] X. He, L. Wang, X. Chen, *J. Appl. Polym. Sci.* **2001**, *80*, 1571.
[21] J. Feng, C. Chan, *Polymer* **2000**, *41*, 7279.
[22] X. Yi, G. Wu, D. Ma, *J. Appl. Polym. Sci.* **1998**, *67*, 131.
[23] H. Jerominek, M. Renaud, N. R. Swart, F. Picard, T. D. Pope, M. Levesque, M. Lehoux, G. Bilodeau, M. Pelletier, D. Audet, P. Lambert, *Proc. SPIE—Int. Soc. Opt. Eng.* **1996**, *2882*, 111.

Large-Area Electric-Field-Induced Colloidal Single Crystals for Photonic Applications**

By *Anand Yethiraj*,* *Job H. J. Thijssen*, *Alan Wouterse*, and *Alfons van Blaaderen*

Materials with a periodic modulation of refractive index on the (sub)-micrometer scale interact strongly with light and can exhibit a photonic bandgap, the optical analogue of the electronic bandgap in semiconductors.[1] Colloidal suspensions of monodisperse micro-spheres that self-organize, analogously to atomic crystals, into periodic structures with the lowest free energy, are promising as three-dimensional photonic materials.[2–6] However, growing large single-domain colloidal crystals without an overlying fluid layer is difficult. We present a technique to grow millimeter-scale (3 mm × 0.5 mm) electric-field-induced colloidal single crystals, and a polymerization process that immobilizes them, allowing drying and reversal of the refractive-index contrast. A 70 $V\,mm^{-1}$ (rms) electric field switches the crystal structure from close-packed to body-centered tetragonal (bct). Lower values increase the area of single-domain close-packed crystals and the preference for face-centered cubic (fcc) packing over hexagonal close-packed (hcp). Intermediate fields produced mixed crystals with a lower fcc layer and a connected upper bct layer.

Most photonic applications require periodic structures with a low filling fraction of the high dielectric-constant component. This can be achieved by preparing wet colloidal crystals with a high particle volume fraction and "inverting the contrast" by drying the crystal, re-infiltrating it with a high-index material, and ultimately removing the solid spheres by etching or burning.[2] High-volume fraction colloidal crystals can be made by allowing colloids in suspension to sediment in gravity and densify. When colloids interact with each other as hard spheres or as slightly charged spheres (with a hard core plus a repulsive inter-particle interaction) the resulting equilibrium structure is an fcc crystal. However, for hard spheres, the

[*] Dr. A. Yethiraj,[+] J. H. J. Thijssen, A. Wouterse, Prof. A. van Blaaderen
FOM Institute for Atomic and Molecular Physics
Kruislaan 407, 1098 SJ Amsterdam (The Netherlands) and
Soft Condensed Matter, Debye Institute, Utrecht University
Princetonplein 5, NL-3584 CC Utrecht (The Netherlands)
E-mail: yethiraj@chem.ubc.ca; A.vanBlaaderen@phys.nu.nl
[+] Present address: Department of Chemistry, 2036 Main Mall, Vancouver, British Columbia, Canada V6T 1Z1, Canada.

[**] We acknowledge useful discussions with Alexander Moroz and Benito Groh, Jacob Hoogenboom for synthesizing the silica spheres, Dirk Vossen for his help in obtaining the SEM images and C. J. Wisman for help with the electronics. This work is part of the research program of the "Stichting voor Fundamenteel Onderzoek der Materie (FOM)", which is financially supported by the "Nederlandse organisatie voor Wetenschappelijke Onderzoek (NWO)". Supporting Information is available online from Wiley Interscience or from the authors.

  DOI: 10.1002/adma.200306192

small free-energy difference between the two close packings[7] often gives rise experimentally to random hexagonal close packing (rhcp), an uncontrolled mixture of fcc and hcp crystal stackings.[8] In addition, colloidal sediments always contain, for entropic reasons, a fluid layer on top, and are thus never completely crystalline.[9,10] An oft-used method, 'controlled drying',[11] uses capillary forces to grow large and complete crystals, but generally produces twinned crystals.[12] For these reasons, preparing large single-domain fcc crystals is challenging and necessitates the use of external fields such as structured bounding surfaces as in colloidal epitaxy,[13] or a flow field.[4] Electric fields have also been used recently: direct current (dc) electrophoresis to accelerate gravitational settling[14] and low-frequency electrohydrodynamics to create close-packed structures in charged colloids,[15] and dielectrophoresis to create two-dimensional crystals.[16] The use of a high-frequency homogeneous external electric field, as presented here, has the advantage that it polarizes only the particle dielectric core and not the double layer, thus working for both charged and uncharged particles, and the field homogeneity results in large millimeter-scale crystals. In addition, variation of the field strength predictably and reversibly switches between two crystal structures (fcc and bct) with different filling fractions and without a colloidal liquid layer on top of the crystal.

In a pure-dielectric fcc crystal, a high dielectric contrast ($\delta = \varepsilon_{max}/\varepsilon_{min} > 8$) at optical frequencies and an "inverse lattice" ($\varepsilon_{medium} > \varepsilon_{spheres}$) configuration are required to open a photonic[17] bandgap. A bandgap is also possible for pure-dielectric inverse bct crystals,[18] but only at $(\varepsilon_{medium}/\varepsilon_{spheres}) > 15.7$. Restrictions on crystal symmetry dictated by these contrast requirements are less strict, however, for metallo-dielectric structures.[19] Moreover, there exist applications such as photonic sensors,[6] where a stop gap is all that is required. For most applications, a thickness of 10 lattice constants is sufficient,[20] but a macroscopic lateral extent is beneficial.

We recently reported a novel field-reversible fcc–bct solid–solid phase transition[21] in a colloidal suspension of fluorescent-labeled silica spheres (radius $r = 702$ nm) in a refractive-index-matching water–dimethylsulfoxide solvent mixture. In the current work, we demonstrate that we can use this reversible martensitic transition to grow large crystals using a procedure that involves annealing defects by repeated sedimentation while ramping the electric field. Because the bct structure is not close-packed, we also invented a new procedure to invert it without loss of structure. Large single-domain field-aligned crystals were made as follows. The electric field was applied between two electrode wires (1.25 mm apart). During colloidal sedimentation it was ramped up in five steps. Prior to each increase in field, the sample was turned over for 10 s (during which the field was turned off). The maximum field in the middle of the sample was calculated to be $E_{rms} = 70\ V\,mm^{-1}$. This repeated sedimentation, while not an optimized procedure, was seen in this work to successfully anneal out defects in the structure, and increase both crystallite size and the orientational correlation between different crystallites.

We characterized the structure by three-dimensional position determination of sphere centers using confocal microscopy, particle-tracking image processing, laser diffraction, and scanning electron microscopy; see references[22,23] for more details. Figure 1A is a 42 μm × 22 μm region of a two-dimensional (2D) *xy* optical slice of the bottom hexagonal close-

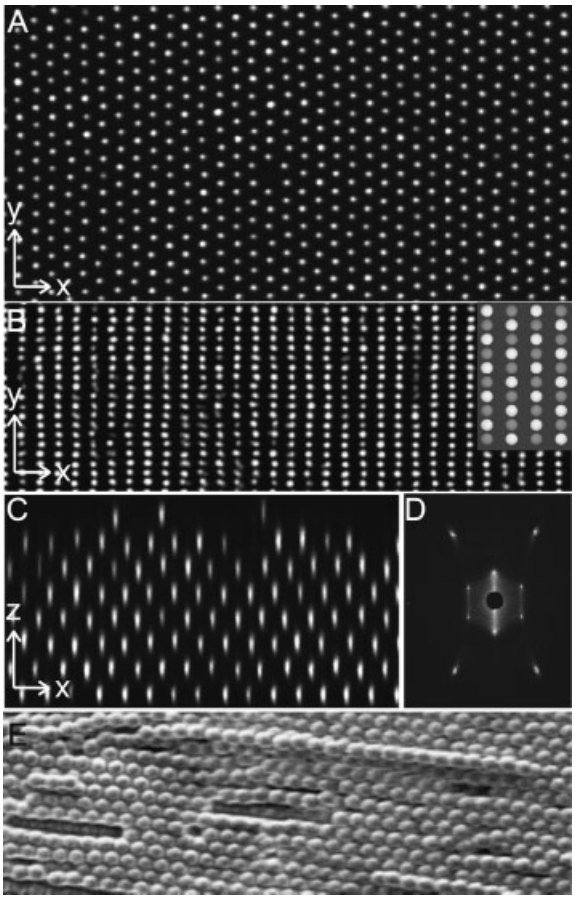

Figure 1. A seven-layer electric-field-induced bct crystal. A) An *xy* optical slice ($E_{rms} = 70\ V\,mm^{-1}$ is along *y*; gravity is along *z*) of an in-focus hexagonal (110) plane. Neighboring spheres touch, but only the fluorescent cores are visible. B) A projection of all the hexagonal planes in the bct crystal. When the images of two adjacent hexagonal close-packed layers are overlaid, the symmetry of this two-layer projection (TLP) is directly linked to the 3D structure, exhibiting rectangular symmetry, while those of close-packed crystals (not shown here) exhibit the higher six-fold symmetry. The inset shows two model hexagonal planes that have been overlaid, with gray and white spheres corresponding to different hexagonal layers, and the circles drawn smaller; at actual size adjacent gray spheres (and white spheres) would be touching. The stacking in a bct lattice is such that adjacent layers are only shifted (by half a lattice spacing) along the direction of the electric field. C) An *xz* scan shows the two-layer periodicity in stacking. Thus, the projection of the entire crystal along the *z*-direction in a bct crystal is identical in symmetry to the two-layer projection (TLP). D) A laser diffraction picture (beam diameter 1 mm) of a pre-polymerized bct crystal shows the characteristic rectangular symmetry (in a close-packed region the diffraction image always exhibits six-fold symmetry; see Supplementary Information). E) An electron micrograph of a bct crystal that has been immobilized by the slow dissolution and re-polymerization of a two-component epoxy into the water–dimethylsulfoxide medium (and subsequent drying) shows clearly that the bct order is preserved in dry form.

ADVANCED MATERIALS

packed plane of a 7-layer bct crystal grown as described above (the electric field is along y and gravity along z). Adjacent spheres touch, but only the fluorescent cores are visible. Figure 1B is a projection of all 7 hexagonal planes in the crystal. A model projection (Fig. 1B, inset) shows two adjacent (110) hexagonal-packed planes of touching gray or white spheres (drawn smaller for clarity), respectively, of a bct crystal. The symmetry of the observed projection corresponds well with the model. (When we used low-ionic-strength 16 MΩ cm water, analysis by three-dimensional (3D) particle position determination showed that the crystal was slightly non-tetragonal and in actual fact face-centered orthorhombic, while the crystals were perfectly tetragonal when 2 MΩ cm water was used. This is consistent with the conditions for observation of orthogonal and tetragonal crystals reported recently in a different experimental system.[24])

A slice in the xz plane (Fig. 1C) shows the stacking of the bct (110) planes. The large-area order is again demonstrated in Figure 1D, which shows a He–Ne laser diffraction image. The 1 mm diameter beam was positioned in between the electrode wires. The bct structure shows a rectangular symmetry distinct from the high six-fold symmetry seen in diffraction patterns of fcc or hcp close-packed structures. Diffraction images taken as a function of position in the sample exhibited an orientational correlation that spanned the extent of the sample (3 cm) and was much larger than the extent of one single crystal.

The bct crystal structure is not close-packed and cannot be preserved simply by drying because of its vulnerability to capillary and meniscus forces. We immobilized the "wet crystal" using a polymerization process to create a low-volume-fraction polymer gel strong enough to keep the particles in place while drying. First, we utilized the slow solubility of a two-component epoxy (applied at the sample edges) in the water–dimethylsulfoxide medium. The epoxy dissolved and polymerized in the solution over a period of 7–11 days. This process was limited by diffusion of the monomer components of the epoxy. The remarkable feature of this "pre-polymerization" step is that a polymer network was created slowly enough and was weak enough that polymerization forces did not destroy the bct crystal, and yet strong enough that subsequent drying and refilling with liquids or a polymer did not destroy it. Next, we carefully broke the cell into two halves. One half was used to produce the scanning electron micrograph of the pre-polymerized and dried bct crystal (Fig. 1E): one sees successive (110) lattice planes of a bct crystal.

To demonstrate that we can turn our dried bct crystals into ones with an 'inverse' contrast, we filled the other half of the dried, pre-polymerized cell with the monomer of an UV epoxy (Norland Optical Adhesive NOA 73, viscosity 130 cP). Filling and subsequent polymerization did not perturb the structures. Figure 2A shows single-domain bct order in a projection of in-focus hexagonal planes through the sample bulk. The sample was cured in ultraviolet light while on the microscope stage. We verified the absence of particle motion during this process. Figure 2B shows an image (time-averaged over

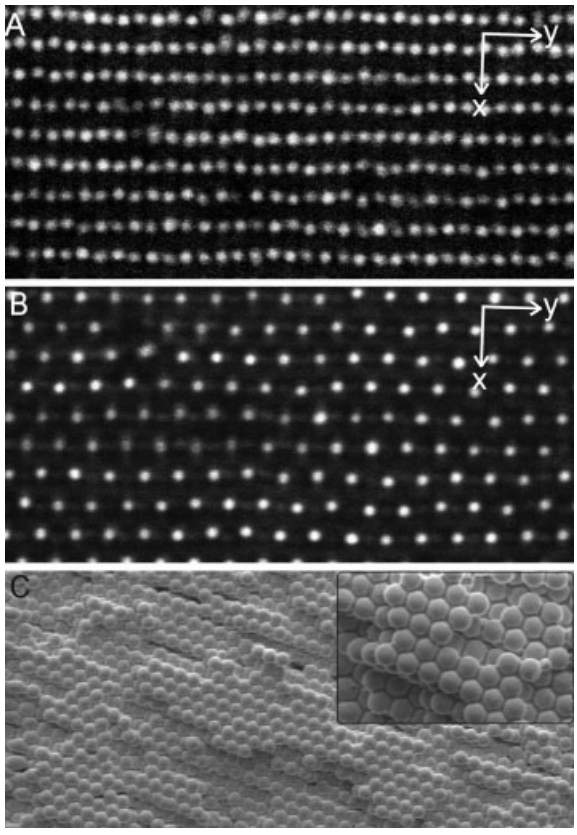

Figure 2. A) On refilling the dried bct sample with UV-curable epoxy, the resulting structure is still bct, as evidenced in the projection of all the hexagonal layers in the crystal. B) The time-average of a single hexagonal plane over 930 s shows that the spheres are indeed stationary. C) SEM images (magnified region in inset) show clearly the characteristic bct stacking with adjacent hexagonal layers shifted by half a lattice spacing in the direction of the bead-chains.

930 s) of an immobile and hence well-resolved in-focus hexagonal close-packed layer after the UV cure. Finally, we removed the top plate of the sample and imaged (Fig. 2C and inset) the immobilized structure of an incomplete layer (originally complete and in the sample bulk but torn apart while taking apart the sample) with a scanning electron microscope (SEM). Spheres in the bct crystal touch along the field direction: they can thus be dissolved by hydrofluoric acid as in the creation of air-sphere fcc crystals.[25] We verified that these crystals were macroscopically ordered by monitoring the symmetry and orientation of laser and white-light diffraction pattern across the sample length (perpendicular to the field): see Figure in Supplementary Information and/or Contents.

An important feature of the field-induced crystals is their complete crystallinity. A sedimented, close-packed colloidal crystal in zero field has a colloidal-fluid layer separating the colloidal crystal from the supernatant medium for entropic reasons. This is shown in the xz (Fig. 3A) and xy (Fig. 3B) optical slices of an fcc crystal (the white rectangle in Fig. 3A is drawn to highlight the abc stacking in fcc). On increasing the electric field, the structural change begins with the crystal-

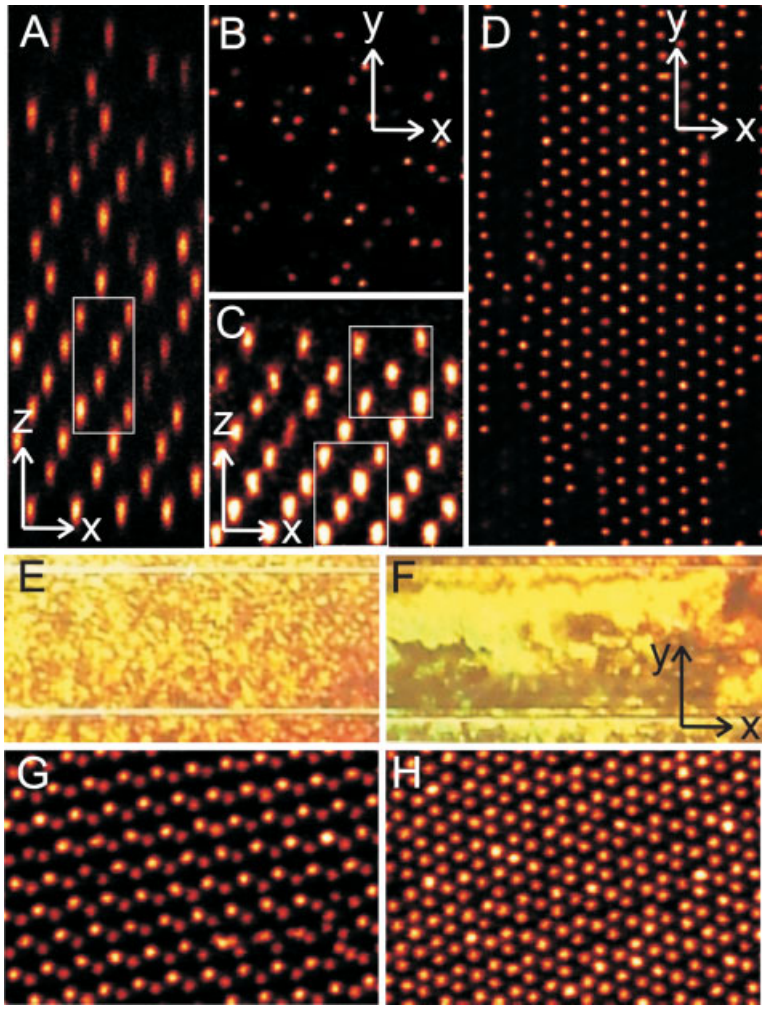

Figure 3. A) *xz* and B) *xy* optical slices: a sedimented, close-packed (fcc) crystal in the absence of an electric field has a colloidal-fluid top layer separating the colloidal crystal, below, from the supernatant medium, above. The white rectangle is drawn to highlight the abc stacking in fcc. C) Mixed crystals at intermediate electric fields: this *xz* optical slice exhibits stacking characteristic of fcc (highlighted by the white rectangle) changing to bct (highlighted by the white square) near the top of the crystal. D) *xy* optical slice: in an electric field, the incomplete top layer is now hexagonal packed. E,F) Images of white-light Bragg reflections of close-packed crystals without and with the field-ramp sample treatment, respectively. White horizontal lines are the electrode wires, spaced 1.25 mm apart. The single domains may be recognized as regions with a single solid-color reflection. G,H) Three-layer projections can distinguish between hcp and fcc close packings. After cycling the field up and down five times, the shown region, initially mostly hcp (G), becomes fcc (H) stacked.

lization of the top layer. The *xz* optical slice (Fig. 3C) shows a mixed crystal with the stacking characteristic of fcc below (highlighted by the white rectangle) changing to bct (highlighted by the white square) near the top of the crystal. Figure 3D shows hexagonal stacking in an incomplete top layer; this layer was fluid-like and disordered at zero field.

For photonic applications, large-area single-domain crystals are desirable. We reproducibly made large fcc single crystals (distinct from polycrystalline regions that exhibit orientational correlations, as noted before) with our method. Images of white-light Bragg reflections of close-packed crystals without and with this sample treatment, respectively, are shown in Figure 3E,F. The single domains may be recognized as regions with a single solid-color reflection: clearly Figure 3F exhibits larger (3 mm × 0.5 mm) single domains. The smaller, 0.5 mm, dimension is probably set by field uniformity dictated by the electrode wire spacing.

While the field-induced structural change was largely reversible, we noticed two irreversible effects. First, the crystallites always oriented such that chains of touching spheres were aligned with the external electric field. Second, repeatedly cycling the field to high and low values made the crystal progressively more fcc. Shown in Figure 3G,H is a three-layer projection that can distinguish between the two degenerate forms of close-packing: hcp (with aba stacking) and fcc (with abc stacking). After cycling the field up and down five times, the region, initially aba stacked, was almost completely fcc (abc stacking). The exact reason for this 'curing' effect, perhaps related to the martensitic fcc–bct transition,[21] is currently under investigation.

We have demonstrated a robust methodology for generating large single-domain crystals that are completely crystalline, millimeter-scale, and of different crystal types: bct, fcc, and mixed fcc–bct. A reproducible recipe was invented to immobilize and dry these structures in order to invert the index contrast. We are currently working with this method to produce inverse silicon bct crystals.[3] The homogeneous external electric field at low field strengths enables the growth of colloidal crystals and at higher fields introduces active control on mixed crystals going from pure fcc to pure bct, and therefore broadens the range of crystal structures accessible to study.

Experimental

Colloids: The colloidal suspension was composed of core–shell silica particles (3 % polydispersity) in a refractive-index-matching liquid mixture of water and dimethylsulfoxide (DMSO) (11.6 % water and 88.4 % DMSO by weight). The spheres have a fluorescent-labeled core of radius, $r = 193$ nm, surrounded by a non-fluorescent shell of thickness 492 nm (transmission electron microscopy). The total radius (static light scattering) was 702 nm. In the absence of an electric field and added salt the interactions are not strictly hard-sphere-like, with the inter-particle spacing $d = (1.0 - 1.06)2R$. However, under the conditions of this experiment but without an electric field, the behavior found for this system was consistent with hard-sphere-like behavior [10]. The core–shell architecture allows three-dimensional position determination without ambiguity even for touching spheres via fluorescent confocal laser scanning microscopy [22].

Sample Preparation: Two strips of 50 μm diameter electrode wire (Goodfellow T2 Thermocouple Alloy Ni95/(Al+Mn+Si)5) were

ADVANCED MATERIALS

placed parallel atop a clean 25 mm × 75 mm × 1 mm microscope slide, 1.1 or 1.25 mm apart, and glued under tension (the gluing points are outside the sample area). Contacts were made to insulated electrical wires using silver epoxy or tin solder. A clean cover slide was placed atop the wires (which thus also served as sample spacers), and glued down at the 4 corners. The edges parallel to the wires were sealed with high-density wax (White Microcrystalline Wax 863, Frank B. Ross Co. Inc.): half a pellet (roughly 3 mm diameter) was placed on each edge and made to carefully fill the sample up to the closest wire by melting the wax, the sample was then filled with the colloidal suspension and the ends glued with the two-component epoxy (Bison Epoxy Rapide; resin is bisphenol-A, average chain length of 2 units; main ingredient of hardener is *N*-(3-dimethylaminopropyl)-1,3-propylenediamine). This ensured a controlled geometry for the subsequent slow dissolution and re-polymerization of the epoxy.

Received: September 17, 2003
Final version: January 5, 2004

[1] a) V. P. Bykov, *Sov. Phys.—JETP* **1972**, *35*, 269. b) E. Yablonovitch, *Phys. Rev. Lett.* **1987**, *58*, 2059. c) S. John, *Phys. Rev. Lett.* **1987**, *58*, 2486. d) *Photonic Crystals and Light Localization in the 21st Century* (Ed: C. M. Soukoulis), Kluwer Academic, Dordrecht, The Netherlands **2001**.
[2] J. E. G. J. Wijnhoven, W. L. Vos, *Science* **1998**, *281*, 802.
[3] Y. A. Vlasov, X. Z. Bo, J. C. Sturm, D. J. Norris, *Nature* **2001**, *414*, 289.
[4] R. M. Amos, J. G. Rarity, P. R. Tapster, T. J. Shepherd, S. C. Kitson, *Phys. Rev. E: Stat., Nonlinear, Soft Matter Phys.* **2000**, *61*, 2929.
[5] A. van Blaaderen, K. P. Velikov, J. P. Hoogenboom, D. L. J. Vossen, A. Yethiraj, R. Dullens, T. v. Dillen, A. Polman, in *Photonic Crystals and Light Localization in the 21st Century, NATO Advanced Study Institute (Crete, Greece 2000)* (Ed: C. M. Soukoulis), Kluwer Academic, Dordrecht, The Netherlands **2001**.
[6] J. H. Holtz, S. A. Asher, *Nature* **1997**, *389*, 829.
[7] S. Pronk, D. Frenkel, *J. Chem. Phys.* **1999**, *110*, 4589.
[8] a) P. N. Pusey, W. Vanmegen, P. Bartlett, B. J. Ackerson, J. G. Rarity, S. M. Underwood, *Phys. Rev. Lett.* **1989**, *63*, 2753. b) Y. A. Vlasov, V. N. Astratov, A. V. Baryshev, A. A. Kaplyanskii, O. Z. Karimov, M. F. Limonov, *Phys. Rev. E: Stat., Nonlinear, Soft Matter Phys.* **2000**, *61*, 5784.
[9] P. V. Braun, P. Wiltzius, *Nature* **1999**, *402*, 603.
[10] J. P. Hoogenboom, D. Derks, P. Vergeer, A. van Blaaderen, *J. Chem. Phys.* **2002**, *117*, 11 320.
[11] P. Jiang, J. F. Bertone, K. S. Hwang, V. L. Colvin, *Chem. Mater.* **1999**, *11*, 2132.
[12] a) K. Wostyn, Y. Zhao, B. Yee, K. Clays, A. Persoons, G. de Schaetzen, L. Hellemans, *J. Chem. Phys.* **2003**, *118*, 10 752. b) K. Wostyn, *Ph.D. Thesis*, University of Leuven **2003**.
[13] a) A. van Blaaderen, R. Ruel, P. Wiltzius, *Nature* **1997**, *385*, 321. b) J. P. Hoogenboom, C. Rétif, E. de Bres, M. van de Boer, A. K. van Langen-Suurling, J. Romijn, A. van Blaaderen, *Nano Lett.* **2004**, *4*, 205.
[14] A. L. Rogach, N. A. Kotov, D. S. Koktysh, J. W. Ostrander, G. A. Ragoisha, *Chem. Mater.* **2000**, *12*, 2721.
[15] a) T. Gong, D. T. Wu, D. W. M. Marr, *Langmuir* **2003**, *19*, 5967. b) W. D. Ristenpart, I. A. Aksay, D. A. Saville, *Phys. Rev. Lett.* **2003**, *90*, 128 303.
[16] S. O. Lumsdon, E. W. Kaler, J. P. Williams, O. D. Velev, *Appl. Phys. Lett.* **2003**, *82*, 949.
[17] a) H. S. Sozuer, J. W. Haus, I. R., *Phys. Rev. B* **1992**, *45*, 13 962. b) A. Moroz, C. Sommers, *J. Phys. Condens. Matter* **1999**, *11*, 997.
[18] R. Tao, D. Xiao, *Appl. Phys. Lett.* **2002**, *80*, 4702.
[19] A. Moroz, *Phys. Rev. B* **2002**, *66*, 115 109.
[20] a) J. F. Bertone, P. Jiang, K. S. Hwang, D. M. Mittleman, V. L. Colvin, *Phys. Rev. Lett*. **1999**, *83*, 300. b) Z. L. Wang, C. T. Chan, W. Y. Zhang, Z. Chen, N. B. Ming, P. Sheng, *Phys. Rev. E: Stat., Nonlinear, Soft Matter Phys.* **2003**, *67*, 016 612.
[21] A. Yethiraj, A. Wouterse, B. Groh, A. van Blaaderen, *Phys. Rev. Lett.* **2004**, *92*, 058 301.
[22] a) A. van Blaaderen, *Adv. Mater.* **1993**, *5*, 52. b) A. van Blaaderen, P. Wiltzius, *Science* **1995**, *270*, 1177.
[23] a) L. Liu, P. S. Li, S. A. Asher, *J. Am. Chem. Soc.* **1997**, *119*, 2729. b) N. Lauinger, M. Pinnow, E. Gornitz, *J. Biol. Phys.* **1996**, *23*, 73. c) L. Goldenberg, J. Wagner, J. Stumpe, B.-R. Paulke, E. Gornitz, *Langmuir* **2002**, *18*, 3319.
[24] A. Yethiraj, A. van Blaaderen, *Nature* **2003**, *421*, 513.
[25] O. D. Velev, A. M. Lenhoff, *Curr. Opin. Colloid Interface Sci.* **2000**, *5*, 56.

Submicrometer Scroll/Tubular Lamellar Crystals of Nylon 6,6**

By *Wenwen Cai*, *Christopher Y. Li*,* *Lingyu Li*, *Bernard Lotz*, *Mimi Keating*, and *David Marks*

Nanotubular structures have been the focus of great attention since the discovery of carbon nanotubes (CNTs) in 1991.[1] A number of nanotubular solids, including carbon and gallium nitride, have been successfully produced.[2–4] Two typical methods have been used to synthesize nanotubular structures: self-assembly and templating techniques. The growth of CNTs can be considered as a self-assembly process. Using ordered porous alumina and oxidized macroporous silicon with narrow pore size distributions as templates, polymeric materials (e.g., polytetrafluoroethylene, PTFE) have been infiltrated into the cylindrical pores. Removal of the templates has led to the creation of polymeric tubular structures with a diameter of 300 nm and wall thickness of 20–50 nm.[5] In the case of single-walled carbon nanotube (SWNTs), the tube wall is a single layer of graphene sheet and the tube diameter is less than 10 nm. In contrast to SWNTs, template-generated polymeric nanotubes possess larger diameters and the tube walls are

[*] Prof. C. Y. Li, L. Li
Department of Materials Science and Engineering, Drexel University
Philadelphia, PA 19104 (USA)
E-mail: Chrisli@drexel.edu
W. Cai
Department of Polymer Science, The University of Akron
Akron, OH 44325 (USA)
Dr. B. Lotz
Institute Charles Sadron
6 Rue Boussingault, Strasbourg, France 67083 (France)
Dr. M. Keating, Dr. D. Marks
Experimental Station, DuPont Central Research & Development,
Wilmington, DE 19880 (USA)

[**] This work was supported by the National Science Foundation (NSF CAREER award, DMR-0239415), ACS-PRF, and 3M Corporation. This work was initiated at the University of Akron and was carried out at Drexel University. CYL is grateful to Prof. S. Z. D. Cheng, Dr. F. Khoury, and Prof. P. Geil for their continuous support and enthusiastic discussions.

  DOI: 10.1002/adma.200305634